Bio-Design and Manufacturing (2023) 6:405–422
https://doi.org/10.1007/s42242-023-00231-9

RESEARCH ARTICLE

Enhancement of intranasal mucosal immunization of mucosal vaccines by ultrasonic treatment

Haowei Xu[1] · Yang Liao[2] · Mankovskaya Svetlana[3] · Deguang Yang[4] · Huaibin Wan[4] · Zonghua Liu[1]

Received: 2 June 2022 / Accepted: 3 January 2023 / Published online: 24 March 2023

Abstract

The pathogens of most infectious diseases invade the host through mucosal sites, and immunization with mucosal vaccines is the best means of combating these infectious diseases. Oral delivery and nasal delivery are the most common methods of mucosal vaccination. However, the delivery process is inefficient, and mucosal vaccination is ineffective because the vaccine formulation is easily and rapidly removed and has difficulty in crossing the mucosal surface. In this paper, we investigated whether the mucosal immune response could be enhanced by ultrasound facilitation of nasal mucosal delivery of vaccine preparations. For this purpose, we used manganese dioxide (MnO_2) as the vaccine carrier/adjuvant, coated with chitosan oligosaccharide (COS) to enhance mucosal adsorption, and further physically adsorbed model antigen ovalbumin (OVA) to construct a nanoparticulate vaccine formulation MnO_2@COS@OVA. Ultrasound treatment was found to promote antigen delivery and recruitment of dendritic cells (DCs) and macrophages as well as T-cell infiltration in nasal mucosal tissues through nasal mucosal immunization studies. With ultrasound assistance, MnO_2@COS@OVA particles promoted the maturation of DCs in vitro and in vivo and promoted the production of effector memory T cells in vivo and cytokine secretion by splenocytes in vitro. In particular, ultrasound treatment significantly increased the levels of secretory IgA antibodies in the nasal mucosa and genital tract mucosa of experimental mice. In addition, the experimental data showed that the MnO_2@COS@OVA particles had good biocompatibility and caused no significant damage to the nasal mucosal and vital organ tissue. These data suggest that ultrasound treatment can promote the induction of efficient immune responses to mucosal vaccines and provide new ideas for the opening and clinical translation of mucosal vaccines.

Haowei Xu and Yang Liao have contributed equally to this work and should be considered as co-first authors.

✉ Huaibin Wan
docvanhb@outlook.com

✉ Zonghua Liu
tliuzonghua@jnu.edu.cn

1 Department of Biomedical Engineering, Jinan University, Guangzhou 510632, China

2 Department of Laboratory Medicine, General Hospital of Southern Theatre Command of PLA, Guangzhou 510010, China

3 Institute of Physiology of NAS of Belarus, Minsk, Belarus

4 Department of Cardiology, Heyuan Shenhe People's Hospital, The Fifth Affiliated Hospital, Jinan University, Heyuan 517475, China

Graphic abstract

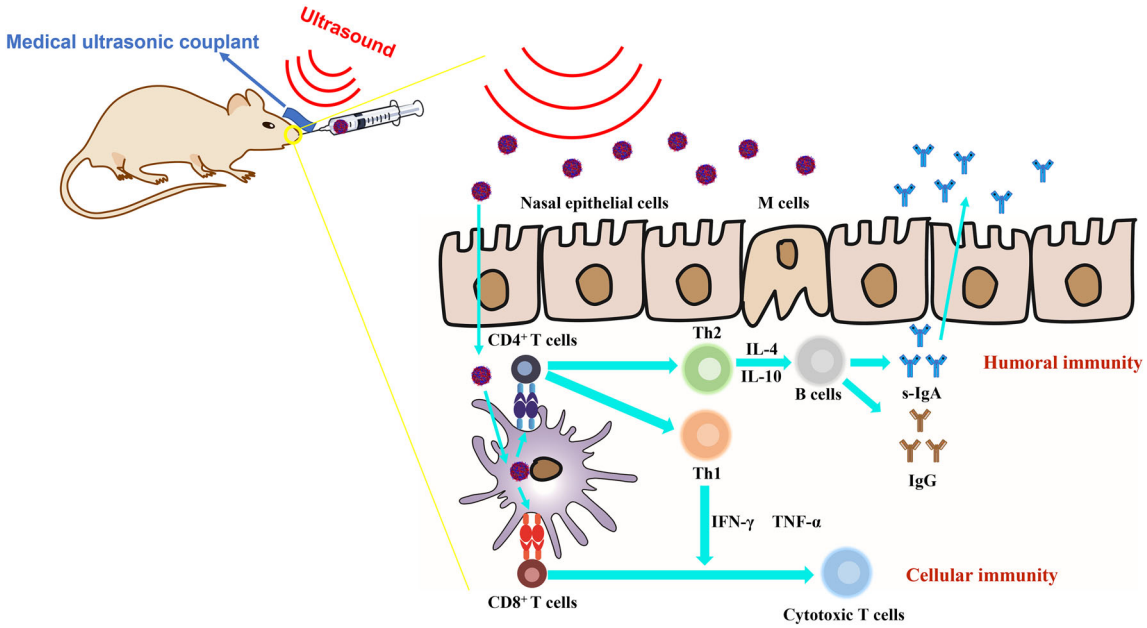

Keywords Mucosal vaccine · Ultrasound treatment · MnO_2 · Nasal delivery

Introduction

It is estimated that 70% of pathogens invade their hosts through mucosal sites [1]. The mucosal immune system, as the first immune barrier in the body, possesses a higher concentration of antibodies than other tissues in the body and protects against more than 90% of potential pathogens [2]. Mucosal vaccination is the best means to protect against pathogens that invade mucosal sites. However, to date, a vast majority of vaccines for infectious diseases approved for marketing have been administered via the nonmucosal route. These vaccines induce an effective systemic immune response but not an effective mucosal immune response [3, 4]. The reason for this is that vaccine delivery at the mucosal site is inefficient and fails to induce an effective mucosal immune response due to the rapid clearance of the vaccine formulation and the difficulty in crossing the mucosal surface. For this reason, researchers have adopted various strategies to enhance the delivery of mucosal vaccines. Currently, mucosal vaccines can be broadly classified into two categories. One category is the use of attenuated or inactivated viruses and bacteria as antigenic vectors to enhance mucosal vaccine delivery through the autonomous invasion ability of these pathogens, such as adenovirus vectors and lactic acid bacteria vectors [5, 6]. The other category is the use of biomaterials as carriers to enhance the transmucosal delivery of vaccines by using their unique physicochemical properties (e.g., electrostatic adsorption), such as liposomes and squalene nanoemulsions [7, 8]. However, at present, the number of safe and effective mucosal vaccines is extremely small and far from sufficient to meet the widespread clinical demand for mucosal vaccines.

The route of delivery is an important factor affecting the efficacy of mucosal vaccination, with oral delivery and nasal delivery being the most common [3, 9]. However, oral delivery faces multiple challenges, especially the protein hydrolases in the gastrointestinal tract and the acidic pH environment that tend to degrade antigens [10]. Compared to other mucosal vaccine delivery routes, antigen degradation is significantly reduced in nasal delivery, and a large number of immune cells are located in the nasal region, the surface layer of the nasal mucosa relatively easy to penetrate [11]. In addition, nasal delivery is a needle-free injection and can be performed by unskilled personnel [12]. Despite these multiple advantages of nasal delivery, only a few nasal vaccines have been approved for marketing. This is because there are still many problems in the development of nasal vaccines: low uptake of soluble antigens by nasal immune cells, short residence time due to rapid removal of antigens by cilia in the nasal cavity, poor antigen stability, and insufficient antigen delivery [3].

In the present study, we envisioned whether mucosal immune responses could be enhanced by ultrasound treatment to facilitate nasal mucosal delivery of vaccine formulations. Ultrasound is a mechanical sound wave that vibrates periodically [13] and has been widely used in medical imaging for diagnosis and for drug delivery [13–15], including chemotherapy drugs, hydrocortisone, salicylic acid, oligonucleotides, insulin, and vaccines [16]. It has been reported in the literature that granular substances can move under the action of ultrasound [17], which can be used to facilitate the penetration of antigens into the surface layer of mucous membranes. Moreover, ultrasound can change the cell membrane permeability [18] and is expected to enhance the efficiency of antigen entry into the cell. It has also been shown that ultrasound-driven carriers can deliver antigens to the cytoplasm to produce cross-presentation and promote cellular immune responses [19]. In addition, ultrasound has been found to trigger inflammatory responses and play an adjuvant role in the mucosal immune response [20, 21], as well as to promote the recruitment of dendritic cells (DCs) and macrophages [22, 23]. These studies suggest that ultrasound is expected to enhance the immune response induced by mucosal vaccines through delivery and adjuvant effects.

To this end, we constructed an intranasal mucosal nanovaccine formulation to explore whether ultrasound can promote nasal mucosal delivery of the vaccine and enhance the mucosal immune response. In recent years, the application of manganese dioxide (MnO_2) nanoparticles as vaccine carriers and adjuvants has attracted widespread attention. The MnO_2 material can degrade to harmless water-soluble Mn^{2+} in vivo and thus has good biocompatibility [24]. Second, MnO_2 nanoparticles can load and deliver antigens and have carrier functions. In addition, Mn^{2+} generated from MnO_2 degradation has an adjuvant effect and can enhance the immune response of the body [25]. Accordingly, we selected MnO_2 as a vaccine carrier/adjuvant. However, MnO_2 nanoparticles are negatively charged and have electrostatic repulsion with the identically charged antigen and mucosal surface layer, which is not conducive to antigen loading and transmucosal delivery. To overcome this drawback, we coated the MnO_2 surface with chitosan oligosaccharide (COS), a chitosan degradation product with good biocompatibility and biodegradability, to prolong the vaccine residence time by electrostatic attraction with the mucosal surface [26–28]. Moreover, COS can open the cellular gap of the mucosal surface layer and promote mucosal uptake while improving the efficiency of mucosal delivery of antigen [29]. On this basis, the obtained MnO_2@COS nanoparticles were further physically adsorbed with the model antigen ovalbumin (OVA) to construct a nanoparticulate vaccine formulation MnO_2@COS@OVA, which was used to investigate whether ultrasound treatment could promote nasal mucosal vaccine delivery and immunization effects. The data obtained in this study provide an important basis for the use of ultrasound to improve mucosal vaccine immunization.

Materials and methods

Materials

Ethyl orthosilicate and ethanol were purchased from Shanghai Macklin Biochemical Technology Co. (Shanghai, China). Potassium permanganate was purchased from Guangzhou Chemical Reagent Factory (Guangzhou, China). Concentrated ammonia was purchased from Tianjin Damao Chemical Reagent Factory (Tianjin, China). Mucin was purchased from Shanghai Yuanye Bio-Technology Co. (Shanghai, China). A bicinchoninic acid assay (BCA) protein concentration assay kit (enhanced) was purchased from Shanghai Beyotime Biotechnology Co., Ltd. (Shanghai, China). OVA-Cy5.5 was purchased from Three Arrows Biotechnology Co. (Tianjin, China). All flow cytometry antibody dyes and cytokine detection enzyme-linked immunosorbent assay (ELISA) kits were purchased from BioLegend (CA, USA). The Roswell Park Memorial Institute (RPMI) 1640 cell culture medium, fetal bovine serum and penicillin–streptomycin double antibodies were purchased from Gibco (CA, USA). Mouse granulocyte-macrophage colony-stimulating factor (GM-CSF) and mouse interleukin-4 (IL-4) were purchased from PeproTech (NJ, USA). All C57BL/6 female mice (4–6 weeks old) were purchased from HFK Laboratory Animal Technology (Beijing, China). In addition, all animal experiments in this study followed animal ethics and Jinan University guidelines.

Preparation and characterization of MnO_2@COS@OVA

MnO_2 was prepared as described in the literature [24]. First, solid silica nanoparticles (SiO_2) were synthesized according to the method reported in the literature [30]. Then, 4.5 mL of ethyl orthosilicate, 9 mL of 28% concentrated ammonia, 62 mL of ethanol, and 24.5 mL of deionized water were mixed and stirred at room temperature for 2 h. The precipitate was collected by centrifugation at 8000 r/min for 10 min and washed with ethanol and deionized water twice each. Aqueous potassium permanganate solution (containing 300 mg of potassium permanganate) was added to the SiO_2 suspension (containing 40 mg of SiO_2) under sonication, sonicated for 1 h, and stirred at room temperature for 6 h. The mixture was centrifuged at 10 000 r/min for 10 min, the precipitate was collected, and the sample was washed with deionized water three times. The resulting mesoporous MnO_2-coated SiO_2 was added to a 2 mol/L aqueous sodium bicarbonate solution and stirred at 60 °C for 12 h. The mixture was centrifuged

at 10 000 r/min for 10 min, and the precipitate was collected and washed with deionized water three times to obtain hollow mesoporous MnO_2 nanoparticles. Two milliliters of MnO_2 suspension (2 mg/mL) was added to 4 mL of COS solution (1 mg/mL) under ultrasonication and stirred at room temperature for 2 h. The mixture was centrifuged at 8000 r/min for 10 min, and the precipitate was collected and washed twice with deionized water. The 500 μL MnO_2@COS suspension (containing 1 mg MnO_2@COS) was mixed with 500 μL OVA solution (containing 300 μg OVA) and incubated at room temperature for 168 h. The supernatant was centrifuged at different time points, and the OVA content in the supernatant was determined by a BCA protein concentration assay kit to calculate the OVA loading. After that, the 500 μL MnO_2@COS suspension (containing 3 mg MnO_2@COS) was comixed with 500 μL OVA solution (containing 300 μg OVA) and incubated at room temperature for 6 h to obtain the vaccine preparation MnO_2@COS@OVA pellets.

The structural composition of five substances (OVA, COS, MnO_2, MnO_2@COS, MnO_2@COS@OVA) was analyzed by Fourier infrared spectroscopy (FT-IR, VERTEX70, Germany). Transmission electron microscopy (TEM, JEM-2010HR, Japan) was used to observe the morphology of MnO_2, MnO_2@COS, and MnO_2@COS@OVA nanoparticles. The zeta potentials of different particles (MnO_2, MnO_2@COS, MnO_2@COS@OVA) were determined using a Malvern laser nanoparticle sizer (Zetasizer Nano ZS, Malvern Instruments Ltd., UK) with a test sample concentration of 0.05 mg/mL.

Functional characterization of MnO_2@COS@OVA and its components

Five hundred microliters of COS solution (containing 3 mg of COS) was mixed with 500 μL of OVA-Cy5.5 solution (containing 300 μg of OVA-Cy5.5) and incubated for 6 h at room temperature to obtain COS@OVA-Cy5.5. Six 4- to 6-week-old C57BL/6 female mice were randomly divided into two groups, and they were administered OVA-Cy5.5 and COS@OVA-Cy5.5 via the intranasal route (administration dose was 40 μL, OVA-Cy5.5 content was 300 μg/mL). At different time points (1, 6, and 12 h), the fluorescence intensity of the nasal cavity was observed by an in vivo imaging system (IVIS, PerkinElmer, FX Pro, Bruker, USA).

A DC cell line (DC2.4) was inoculated into 24-well cell culture plates (each well contained 1×10^6 cells). The cells were divided into three groups (Control, MnO_2, MnO_2@COS), where the content of MnO_2 was 1.5 mg/mL. The cells were placed at 37 °C with 5% carbon dioxide (CO_2) and coincubated with the material for 24 h. The cell suspension was centrifuged (1000 r/min, 5 min), and the supernatant was collected. The supernatant was stored at −80 °C and used for the IFN-β assay. The level of IFN-β secretion in the supernatant was measured by an ELISA kit.

Effect of ultrasound treatment on cross-mucus delivery of MnO_2@COS@OVA particles

The nasal mucus composition was as described in the literature [31]. We dissolved 2.5 mg of mucin in 10 mL of deionized water to obtain a mucin solution to simulate nasal mucus. A hydrogel was made by dissolving 0.02 g of sodium alginate with 0.05 g of calcium chloride in 10 mL of deionized water. The resulting mucin solution was coated on the surface layer of the hydrogel to simulate the surface layer of the nasal mucosa. Two hundred microliters of MnO_2@COS@OVA suspension (1 mg/mL) was added to two groups (MnO_2@COS@OVA group, MnO_2@COS@OVA+US group), each consisting of 4 mL of mucin solution with 5 mL of hydrogel. The MnO_2@COS@OVA group was placed naturally for 5 min, and the MnO_2@COS@OVA+US group was treated with ultrasound (the NSE-UPH-I handheld ultrasonic acoustic power processor (Nason Ultrasound, Suzhou, China)) at an ultrasound frequency of 1 MHz, a power density of 0.48 W/cm^2, and an ultrasound time of 5 min (stopping for 5 s every 5 s of work) according to previously reported experience with ultrasound parameters [19–21, 23, 32]. Subsequently, the hydrogel surface was rinsed twice with deionized water to remove mucin and free particles. Particle retention in the hydrogels of both groups was observed with a microscope (DMRA2, Leica, Germany).

Effect of ultrasound treatment on bone marrow-derived dendritic cells (BMDCs)

BMDCs were extracted by referring to the literature [33]. BMDCs were generated from the bone marrow cells of C57BL/6 mice (female, 4–6 weeks old). First, the mice were anesthetized, killed, and immersed in 75% (volume fraction) ethanol for 15 min. The femurs and tibias of the mice were excised intact, and the muscles were carefully removed. The bones were soaked in 75% (volume fraction) ethanol for 3 min and washed with phosphate buffered saline (PBS) three times. Then, both ends of the bones were cut, and the bone cavities were rinsed with RPMI 1640 medium by syringe. The obtained marrows were dispersed by vigorous pipetting, and the suspension was filtered through a 200-mesh sieve. The bone marrow cells were collected and cultured in 10 mL RPMI 1640 medium with 10% fetal bovine serum (FBS), 100 IU/mL penicillin, 100 mg/mL streptomycin, 10 ng/mL granulocyte-macrophage colony stimulating factor (GM-CSF) and 5 ng/mL IL-4 in an incubator with a 5% CO_2 atmosphere at 37 °C. Half of the culture medium was changed every two days. After

seven days, the immature BMDCs were harvested and used for further experiments. Immature BMDCs were inoculated into 24-well low-adsorption plates (each well contained 1×10^6 cells). The cells were divided into three groups (OVA, MnO_2@COS@OVA, MnO_2@COS@OVA+US), and the three groups were stimulated with OVA, MnO_2@COS@OVA, and MnO_2@COS@OVA for 24 h. The MnO_2@COS@OVA+US group was sonicated (same conditions as above). Subsequently, BMDCs from different groups were stained for 30 min with the following fluorescently labeled antibody reagents: APC-anti-CD11c, FITC-anti-CD80, Cy5.5-anti-CD40, PE-anti-MHC II and PE-anti-MHC I (in this paper, the PE-anti-MHC I used in the full text is PE anti-mouse H-2Kb specifically bound to the SIINFEKL antigenic peptide of OVA). Subsequently, the expression levels of costimulatory molecules on the surface of BMDCs were analyzed by flow cytometry (Beckman Coulter, USA).

Tissue section to observe nasal mucosa tissue

Fifteen female C57BL/6 mice aged 4–6 weeks were randomly divided into five groups (PBS, PBS+US, OVA, MnO_2@COS@OVA, MnO_2@COS@OVA+US) and administered different vaccine preparations and treatments (40 μL vaccine preparation) by the nasal drip route. Twenty-four hours later, nasal tissues were surgically removed. The resulting tissues were fixed in 4% paraformaldehyde for 48 h and decalcified for 30 days. The decalcified tissues were paraffin-embedded and sectioned. The sections were subjected to immunofluorescence staining (fluorescence-labeled antibody reagents: Cy3-anti-CD11c, FITC-anti-CD68) and hematoxylin-eosin (HE) staining. Microscopic observation of DC and macrophage recruitment in nasal mucosal tissues and nasal mucosal tissue damage was performed. Subsequently, three sets of sections containing OVA were immunohistochemically stained for microscopic observation and analyzed for OVA antigen delivery efficiency. In addition, six female C57BL/6 mice aged 4–6 weeks were randomly divided into two groups, both administered by the nasal drip route with MnO_2@COS@OVA (administered at a dose of 40 μL). The MnO_2@COS@OVA+US group was sonicated (same conditions as above). Seven days later, nasal mucosa tissue sections were obtained by the above method and subjected to immunofluorescence staining (fluorescent labeled antibody reagent: Cy3-anti-CD3). The infiltration of T cells in the nasal mucosa tissue was observed by microscopy.

Immunization of mice

Twenty-five female C57BL/6 mice aged 4–6 weeks were randomly divided into five groups. Four groups were nasal drip groups: OVA, Alum@OVA, MnO_2@COS@OVA, and MnO_2@COS@OVA+US. Each mouse was administered by the nasal drip route (40 μL vaccine preparation), with the MnO_2@COS@OVA+US group undergoing ultrasound treatment for 5 min (conditions as above). The remaining group was the subcutaneous vaccination group (MnO_2@COS@OVA-SC), where each mouse was administered by the subcutaneous route (40 μL of vaccine preparation). OVA (300 μg/mL) was administered to all five groups, with the first vaccination recorded on day 0, followed by a booster on days 7 and 11. Mice were executed 4 days after the last vaccination, and splenocytes, blood, nasal lavage, and genital tract lavage were collected.

In vivo DC activation

Mouse spleens were removed, washed, ground, and centrifuged (1000 r/min, 5 min), and splenocytes were collected. Blood cells were removed with erythrocyte lysate and centrifuged (1000 r/min, 5 min), and splenocytes were collected, resuspended and counted in RPMI 1640 complete medium, diluted to 1×10^7 cells/mL, and stored as splenocyte stock solution. One hundred microliters of splenocyte master mix was taken and stained for 30 min with the following fluorescently labeled antibody reagents for different groups of splenocytes: APC-anti-CD11c, FITC-anti-CD80, Cy5.5-anti-CD40, PE-anti-MHC II and PE-anti-MHC I. Subsequently, the expression levels of costimulatory molecules on the surface of $CD11c^+$ splenocytes were analyzed by flow cytometry.

Antibody titer assay

Blood samples, nasal lavage, and genital tract lavage were collected. The blood samples and lavage fluid samples were centrifuged at room temperature, and the supernatant was collected and stored at −20 °C for antibody titer detection. The levels of IgG antibody in serum and IgA antibody titers in mucosal lavage fluid were determined by ELISA kits.

Cytokine assay

Splenocyte stock solution was taken and diluted to a 2×10^6 cells/mL cell suspension. The splenocyte suspension was inoculated into a 6-well plate with 2 mL of splenocyte suspension and 2 mL of OVA solution (OVA concentration of 25 μg/mL, RPMI 1640 complete medium) per well. The cells were incubated at 37 °C with 5% CO_2 for 60 h. The cell suspension was centrifuged (1000 r/min, 5 min), and the supernatant was collected. The supernatant was stored at −80 °C and used for the cytokine assay. The secreted levels of cytokines (IL-4, IL-6, TNF-α, IFN-γ) in the supernatant were measured by ELISA kits.

Memory T-cell assay

Twenty-five female C57BL/6 mice aged 4–6 weeks were randomly divided into five groups. Four groups were nasal drip groups: OVA, Alum@OVA, MnO_2@COS@OVA, and MnO_2@COS@OVA+US. Each mouse was administered by the nasal drip route (40 μL vaccine preparation), with the MnO_2@COS@OVA+US group undergoing ultrasound treatment for 5 min (conditions as above). The remaining group was the subcutaneous vaccination group (MnO_2@COS@OVA-SC), where each mouse was administered by the subcutaneous route (40 μL of vaccine preparation). OVA (300 μg/mL) was administered to all five groups, with the first vaccination recorded on day 0, followed by a booster on days 7 and 14. Mice were killed on day 35, and splenocytes were collected. One hundred microliters of splenocyte stock solution was taken, and different groups of splenocytes were stained with the following fluorescently labeled antibody reagents for 30 min: APC-anti-CD62L, FITC-anti-CD4, CY5.5-anti-CD8a, and PE-anti-CD44. Subsequently, the fractionation and proportion of memory T cells in splenocytes were analyzed by flow cytometry.

HE staining to observe the major organs

The hearts, livers, spleens, lungs and kidneys of mice were surgically collected, and the resulting organs were fixed in 4% paraformaldehyde for 48 h, paraffin-embedded and sectioned. The resulting sections were subjected to HE staining. Microscopy was used to observe major organ damage in vivo.

Statistical analysis

In this study, the results are presented as the mean±standard deviation. Statistical tests between two groups were performed using a two-tailed *t* test, and statistical tests between multiple groups for the same factor were performed using one-way ANOVA. Significance was determined based on *p* values: $*p<0.05$, $**p<0.01$, and $***p<0.001$.

Results and discussion

Physicochemical properties of MnO_2@COS@OVA

The synthesis path of MnO_2@COS@OVA is shown in Fig. 1a. First, hollow mesoporous MnO_2 nanoparticles were synthesized using silica as a template for vaccine carrier/adjuvant. Next, COS was coated on the surface of MnO_2 to improve its antigen loading and transmucosal delivery ability to obtain MnO_2@COS. Finally, the MnO_2@COS physisorbed model antigen OVA was used to make the vaccine formulation MnO_2@COS@OVA, and the loading of OVA can be seen in Fig. S1 (Supplementary Information). Next, FT-IR was used to analyze the five substances (OVA, COS, MnO_2 MnO_2@COS, MnO_2@COS@OVA) for their structural composition. As shown in Fig. 1c, the absorption peak located at 580 cm^{-1} is the characteristic absorption peak of the Mn–O bond. The absorption peak located at 1150 cm^{-1} is the C–N bond stretching vibration absorption peak. The absorption peaks at 2870 and 1410 cm^{-1} are C–H bond stretching and bending vibration absorption peaks [34]. The absorption peak located at 1652 cm^{-1} is the characteristic absorption peak of protein amide I [35]. The above infrared (IR) spectra indicated that the MnO_2 surface was successfully coated with COS and loaded with OVA. Furthermore, the morphologies of MnO_2, MnO_2@COS and MnO_2@COS@OVA particles were observed by TEM. As shown in Fig. 1b, all three particles are hollow mesoporous spherical structures with a particle size of approximately 350 nm. Subsequently, the zeta potentials of MnO_2, MnO_2@COS, and MnO_2@COS@OVA were measured by nanolaser particle size measurements. The particle size distribution and PdI are shown in Figs. S2a and S2b (Supplementary Information). As shown in Fig. 1d, the zeta potentials of MnO_2, MnO_2@COS and MnO_2@COS @ova are (−34.80±0.36) mV, (14.30±0.81) mV and (−1.21±0.43) mV, respectively.

Functions of MnO_2@COS@OVA and its components

COS is a chitosan degradation product with good biocompatibility and biodegradability. COS is positively charged, which can produce electrostatic attraction with the surface of the mucous membrane and prolong the residence time of the vaccine. To explore whether COS can enhance the residence time of the vaccine, the fluorescence intensity of OVA-Cy5.5 and COS@OVA-Cy5.5 in the nasal cavity at different time points was observed by IVIS. As shown in Figs. 2a and 2b, the residence time of COS@OVA-Cy5.5 in the nasal cavity was significantly longer than that of OVA-Cy5.5. In addition, to investigate whether Mn^{2+} can activate the stimulator of interferon gene (STING) pathway, we determined the amount of IFN-β in the cell supernatant by ELISA. STING is an important intrinsic immune signaling molecule in organisms, and STING promotes the production and release of interferon and inflammatory factors by constituting a specific signal transduction pathway, causing immunity against pathogens [25]. As shown in Fig. 2c, the secretion of IFN-β by DC2.4 in the MnO_2 and MnO_2@COS groups was significantly higher than that in the control group. The above data show that COS can increase the residence time of the vaccine in the nasal cavity and that MnO_2 and MnO_2@COS can be used as adjuvants to activate the STING pathway.

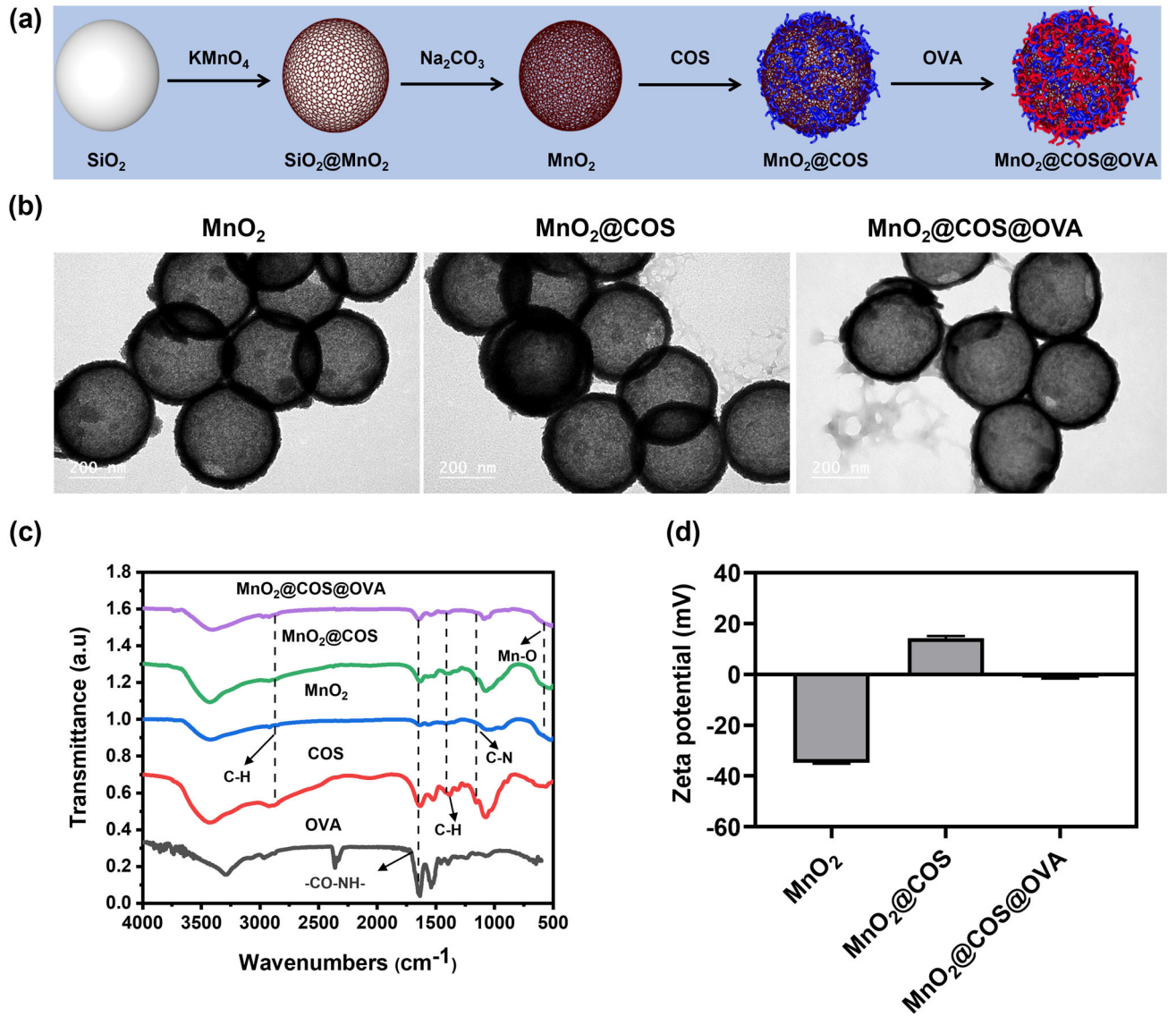

Fig. 1 Design and characterization of vaccines. **a** Schematic diagram showing the synthesis of MnO_2@COS@OVA particles. **b** Transmission electron micrographs of MnO_2, MnO_2@COS, and MnO_2@COS@OVA. **c** Infrared (IR) spectra of five substances, OVA, COS, MnO_2, MnO_2@COS, and MnO_2@COS@OVA. **d** Zeta potential of three particles, MnO_2, MnO_2@COS, and MnO_2@COS@OVA

Effect of ultrasound treatment on the delivery of vaccine formulations across mucus

Mucus secretion consists of mucin, which is negatively charged overall and is produced by the cupped cells in the mucosal epithelium. One of the main functions of mucus is to prevent the invasion of foreign particles (e.g., microorganisms). Therefore, mucus greatly affects the motility and permeability of vaccine formulations [36, 37]. To investigate whether ultrasound treatment can enhance the cross-mucus delivery of MnO_2@COS@OVA particles, a mucin-coated hydrogel surface was used to simulate the surface of the nasal mucosa. MnO_2@COS@OVA was dropped onto this mucin surface and sonicated, the mucus layer was removed, and the content of MnO_2@COS@OVA resting within the hydrogel was observed using microscopy. As shown in Fig. 2d, ultrasound treatment significantly promoted the cross-mucus delivery of this vaccine formulation compared to the control group. This result suggests that ultrasound treatment is expected to enhance the in vivo transmucosal delivery of the vaccine formulation.

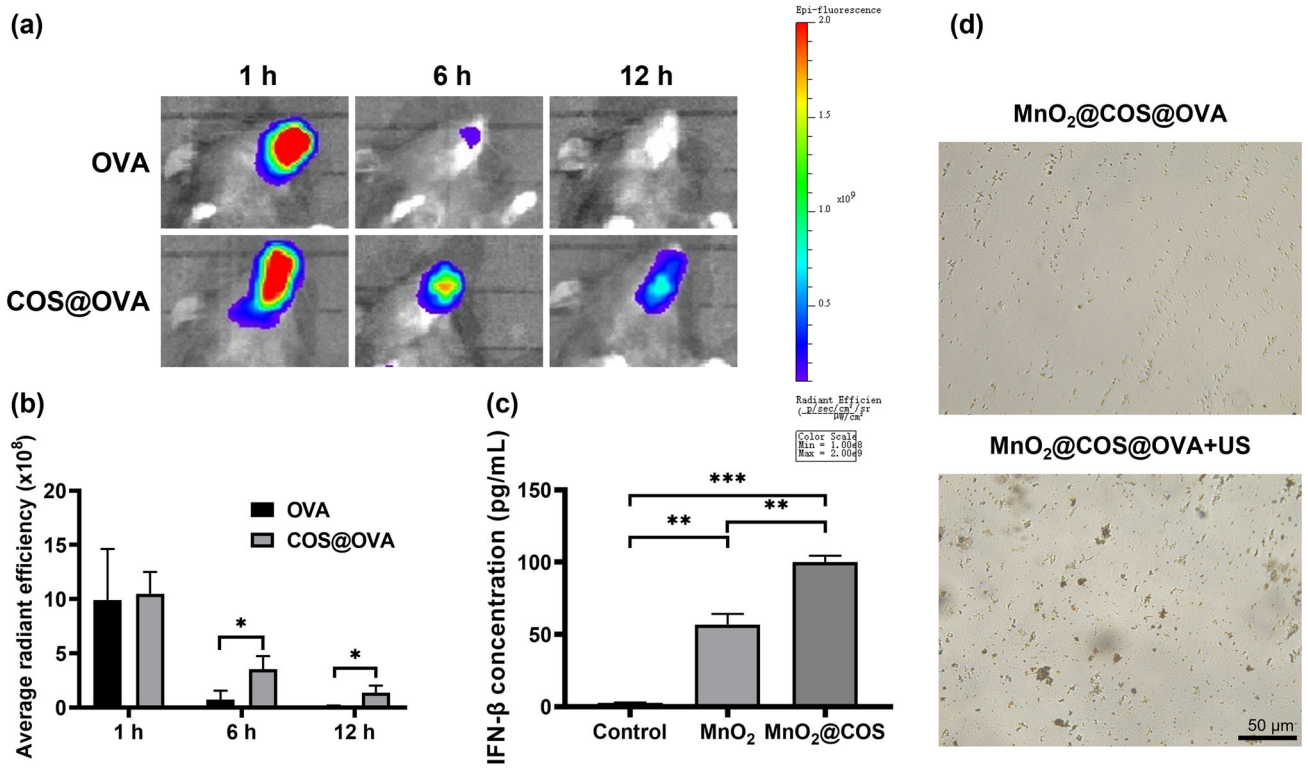

Fig. 2 **a** Typical in vivo imaging system (IVIS) images of the mice at 1, 6 and 12 h after nasal vaccination. **b** Average radiant efficiency around the injection site. **c** Content of IFN-β in the cell supernatants. **d** Number of MnO2@COS@OVA particles residing in the hydrogel. Data represent the mean±standard deviation ($n \geq 3$). $^{**}p<0.01$ and $^{***}p<0.001$ were used to indicate significant differences

Effect of ultrasonically treated vaccine preparations on BMDCs

DCs are antigen-presenting cells (APCs). The maturation of DCs is an important step in generating an effective immune response. Immature DCs are highly capable of capturing antigens, and their antigen processing and delivery capacity increases with cell maturation [38]. High expression of the costimulatory molecules CD40 and CD80 is often a sign of DC maturation. In general, most of the exogenous antigens captured and processed by APCs are delivered to $CD4^+$ T cells via MHC class II molecules, mediating humoral immunity, and some are delivered to $CD8^+$ T cells via MHC class I molecules, mediating cellular immunity via antigen cross-presentation. To investigate the effect of MnO_2@COS@OVA+US on BMDCs, the expression levels of CD80, CD40, MHC II and MHC I on BMDCs were analyzed by flow cytometry. As shown in Figs. 3a–3e, the expression levels of MHC I, CD80 and CD40 were significantly higher in the MnO_2@COS@OVA+US group than in the other two groups. This result is generally consistent with previous reports [19]. This is due to ultrasound treatment promoting cytoplasmic delivery of the vaccine preparation, enhancing antigen cross-presentation and increasing MHC I expression levels. This experiment suggests that ultrasound treatment can assist vaccine adjuvants in promoting the activation of BMDCs and their MHC I expression.

Effect of ultrasonically treated vaccine preparations on APCs in nasal mucosal tissue

Macrophages and DCs are both APCs, and the recruitment of APCs is one of the steps to generate an effective immune response. In some immunotherapy strategies, researchers have used various approaches to recruit APCs (e.g., using adjuvants) to enhance the therapeutic effect [39]. To investigate whether ultrasound treatment can promote the recruitment of DCs and macrophages in vivo, nasal tissues from each group of mice were extracted, tissue sections were made, and immunofluorescence staining was performed for CD11c, a characteristic protein of DCs, and CD68, a characteristic protein of macrophages, in the tissue sections. Figure 4a shows a schematic diagram of ultrasound application. As shown in Fig. 4b, the number of DCs and macrophages in the PBS+US group was greater than that in the PBS group. This indicates that ultrasound treatment can promote the recruitment of DCs and macrophages. Previous

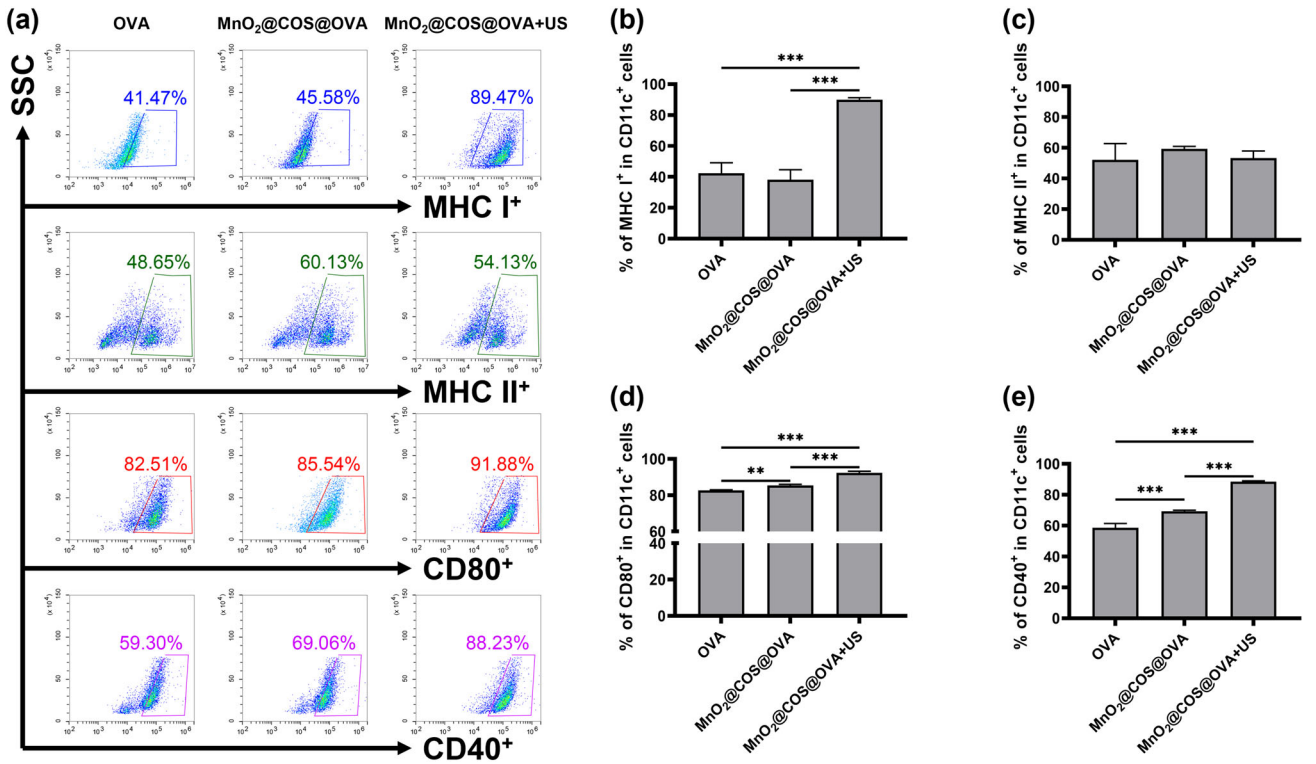

Fig. 3 Effect of ultrasound-treated vaccine preparations on bone marrow-derived dendritic cells (BMDCs). **a** The expression of four molecules, CD80, CD40, MHC II and MHC I, expressed on BMDCs was analyzed by flow cytometry. **b** Expression level of MHC I on BMDCs. **c** Expression level of MHC II on BMDCs. **d** Expression level of CD80 on BMDCs. **e** Expression level of CD40 on BMDCs. Data represent the mean±standard deviation ($n \geq 3$). $^{**}p<0.01$ and $^{***}p<0.001$ were used to indicate significant differences

studies reported that ultrasound treatment can promote the recruitment of DCs in the skin [23]. Another study reported that ultrasound treatment promotes macrophage recruitment by triggering an inflammatory response [22]. In addition, ultrasound treatment alone has been reported to exert adjuvant effects by eliciting an inflammatory response [20]. Figure 4b shows that the number of DCs and macrophages was higher in the MnO_2@COS@OVA+US group than in the OVA group and the MnO_2@COS@OVA group. To investigate whether ultrasound treatment can promote T-cell infiltration in vivo, immunofluorescence staining of CD3, which is the characteristic protein of T cells, was performed in tissue sections. T cells are important immune cells that are distributed in immune organs and tissues throughout the body through lymphatic and blood circulation to perform immune functions. As shown in Figs. 4c and 4d, the number of T cells in the MnO_2@COS@OVA+US group was greater than that in the MnO_2@COS@OVA group. This indicates that ultrasound treatment can promote T-cell infiltration. It has been reported that ultrasound enhances the activation of the STING pathway in APCs and induces T-cell proliferation [21]. This result suggests that ultrasound treatment promotes the recruitment of DCs and macrophages as well as T-cell infiltration in the superficial tissue of the nasal mucosa, contributing to the enhancement of further immune responses.

Damage to the nasal mucosa from ultrasonically treated vaccine preparations

The vaccine formulation delivery process cannot cause significant damage to the surrounding tissues. The inner surface of the nasal cavity is covered with columnar ciliated epithelium with a large number of mucus-secreting cup cells between the epithelium. Nasal toxicity was determined mainly by observing the morphology of nasal mucosal epithelial cells and nasal septal cells. We investigated whether ultrasound treatment and MnO_2@COS@OVA particles caused damage to nasal mucosa tissue. The nasal tissues of each group of mice were extracted, sectioned, and stained with HE to observe the damage caused by ultrasound and the vaccine preparation on the nasal tissues. As shown in Fig. 5a, the morphology of nasal septum cells was normal in all tissues, no obvious epithelial cell detachment was observed, and the morphology of nasal mucosal epithelial cells was clear without cell abnormalities or mucosal disruption. This experiment suggests that the ultrasound-treated

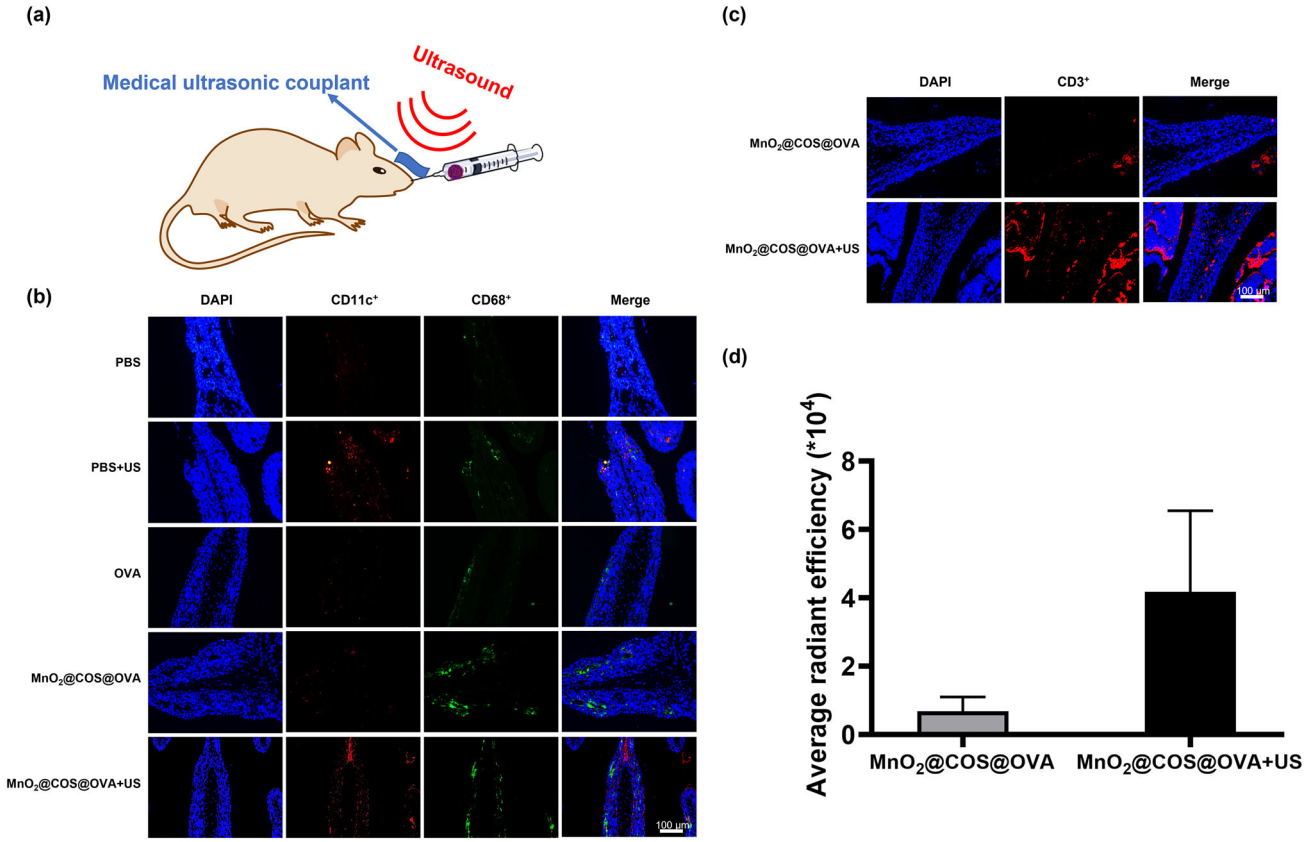

Fig. 4 **a** Schematic diagram of ultrasound application. We applied the ultrasonic coupling agent to the upper skin of the mouse nasal cavity and brought the instrument probe in contact with the ultrasonic coupling agent for ultrasound treatment. The ultrasonic coupling agent is the ultrasonic wave transmission medium. **b** Stained $CD11^+$ molecules (red) and $CD68^+$ molecules (green) in nasal mucosal tissues. **c** Stained $CD3^+$ molecules (red) in nasal mucosal tissues. **d** Average radiant efficiency around the injection site. Data represent the mean±standard deviation ($n \geq 3$)

vaccine preparation does not cause significant damage to the nasal mucosal tissue.

Analysis of the penetration efficiency of ultrasound-treated vaccine preparations on the surface layer of mucosa

Free antigen is readily removed and degraded at the mucosal site. Therefore, vaccine carriers are required to load antigens and deliver them to penetrate the mucosal surface. In this way, the antigen is facilitated to be processed and presented by the large number of APCs under the mucosal surface. We investigated whether ultrasound treatment promotes the penetration of MnO_2@COS@OVA particles into the mucosal surface layer. Immunohistochemical staining of tissue sections was performed to observe the efficiency of antigen penetration into the superficial layers of the nasal mucosa. As shown in Figs. 5b and 5c, the amount of OVA in the nasal mucosa of the MnO_2@COS@OVA+US group was significantly higher than that of the OVA group. This experiment suggests that ultrasound can significantly promote the penetration of vaccine agents into the surface layer of mucosa.

Effect of ultrasonically treated vaccine preparations on DCs in vivo

To further investigate the effect of MnO_2@COS@OVA+US on DCs in vivo, splenocytes were collected and stained with fluorescently labeled antibody reagents. The expression levels of CD80, CD40, MHC II and MHC I on $CD11c^+$ splenocytes were analyzed by flow cytometry. As shown in Figs. 6a–6e, the expression levels of MHC I molecules on $CD11c^+$ splenocytes in the MnO_2@COS@OVA+US group were significantly higher than those of the remaining four groups. The expression levels of MHC II molecules were significantly higher than those in the OVA and MnO_2@COS@OVA groups. The expression levels of CD40 molecules in $CD11c^+$ splenocytes in the MnO_2@COS@OVA+US group were significantly higher than those in the OVA group. This experiment shows that after

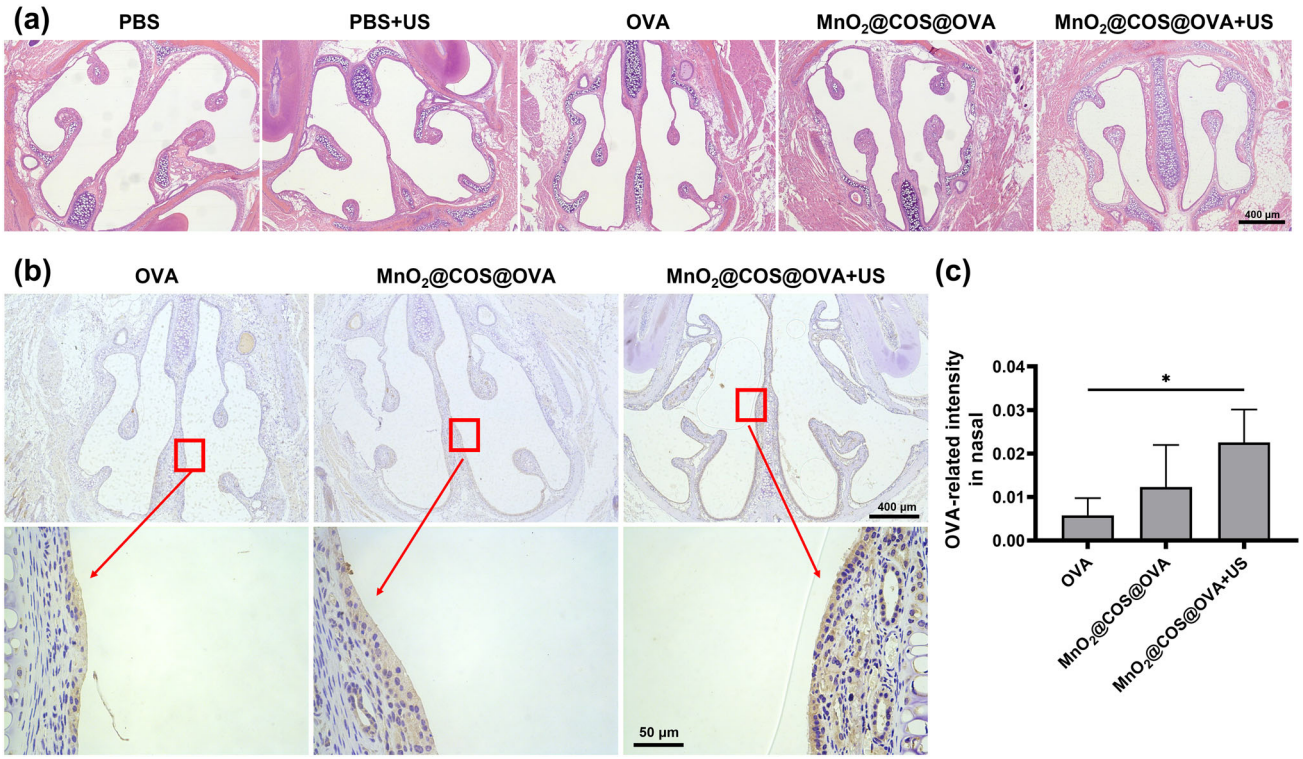

Fig. 5 Ultrasound treatment and vaccine preparation damage the nasal cavity, and ultrasound promotes vaccine preparation penetration of the surface layer of the nasal mucosa. **a** Hematoxylin-eosin (HE) staining map of nasal mucosa showing nasal mucosa injury in five groups (PBS, PBS+US, OVA, MnO_2@COS@OVA, MnO_2@COS@OVA+US). **b** Immunohistochemical staining map of the nasal mucosa of the OVA, MnO_2@COS@OVA and MnO_2@COS@OVA+US groups (n=3). The overall picture at the top and the local magnification circled in the red box below represent the amount of OVA antigen delivery. **c** The ratio of integrated optical density (IOD) to area in the immunohistochemical map is the ratio of the amount of OVA (brown) to tissue area. Data represent the mean±standard deviation ($n\geq3$). *$p<0.05$ was used to indicate significant differences

ultrasonic treatment, MnO_2@COS@OVA particles promote high levels of MHC I and MHC II molecule expression on DCs, which can induce better cellular and humoral immunity.

Antibody potency analysis

Antibody potency is an important indicator of the level of humoral immunity. Moreover, antibody subtype levels can be used to assess the balance of Th1 and Th2 types in helper T cells. The production of IgG1 and IgG2a is associated with Th2- and Th1-type immune responses, respectively [40]. We investigated whether ultrasound-treated vaccine preparations promoted the secretion of IgG-like and IgA antibodies. ELISA kits were used to detect four antibody indicators, IgG, IgG1, IgG2a and IgA. As shown in Figs. 7a–7c, the titers of serum IgG, IgG1 and IgG2a antibodies in the MnO_2@COS@OVA+US group of mice are basically the same as those of the remaining four groups. As shown in Fig. 7d, the values of IgG1/IgG2a in all five groups are between 1 and 1.1, indicating that the induced immune response is a mixed or balanced immune response of Th1 and Th2 [41]. As shown in Fig. 7e, the MnO_2@COS@OVA+US group induced significantly higher IgA secretion from the nasal mucosa than the other four groups. In addition, a significant advantage of mucosal immunity is the ability to induce an immune response in the systemic mucosal immune system. This response not only produces IgA antibodies at mucosal immune sites but also secretes IgA antibodies at distal mucosal sites to protect the host from pathogenic invasion. When antigen activates the mucosal immune system, most of the activated lymphocytes return to the stimulated mucosal site, but some activated lymphocytes move to other mucosal sites, resulting in activation of immune cells in distal mucosal sites [42]. We, therefore, examined the titers of IgA antibodies secreted in the mouse reproductive tract. As shown in Fig. 7f, the MnO_2@COS@OVA+US group induced significantly higher IgA secretion from the genital tract mucosa than the remaining four groups. This indicates that after ultrasound treatment, the vaccine preparation MnO_2@COS@OVA can promote IgA antibody secretion not only from the mucosal immune sites but also from the distal mucosa, thus enhancing the immune response of the

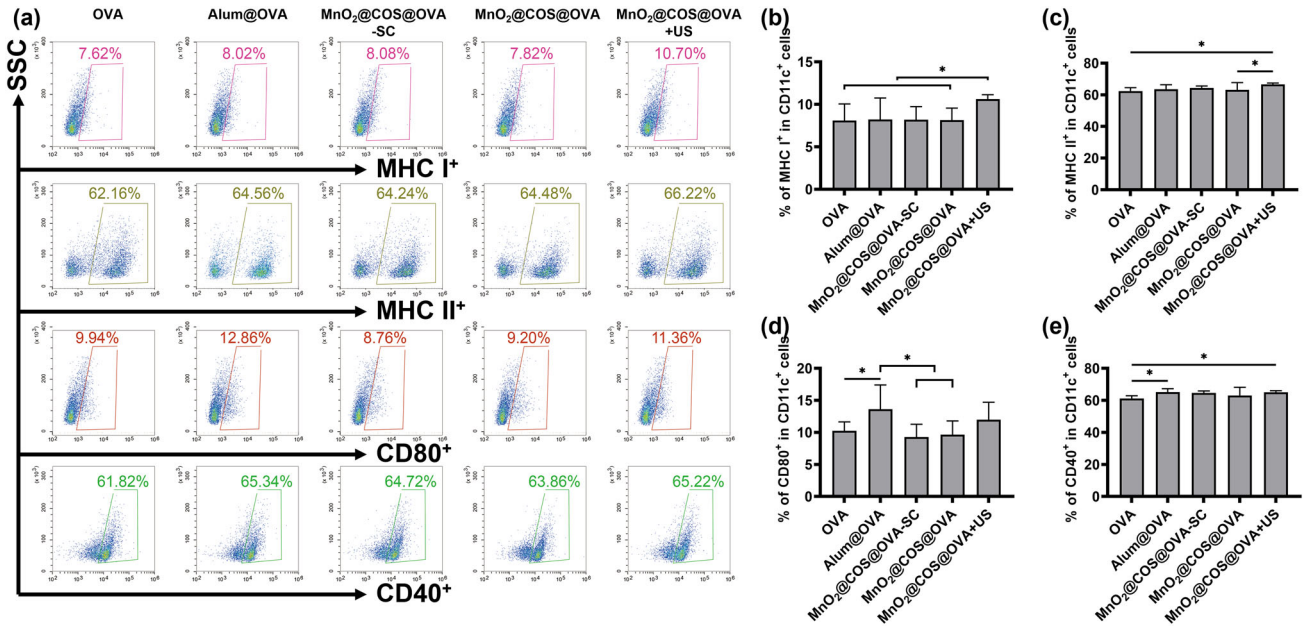

Fig. 6 Effect of ultrasound-treated vaccine preparation on dendritic cells (DCs) in vivo. **a** Expression of four molecules, CD80, CD40, MHC II and MHC I, expressed on DCs cells in splenocytes by flow cytometry. **b** Expression level of MHC I on DCs in splenocytes. **c** Expression level of MHC II on DCs in splenocytes. **d** Expression level of CD80 on DCs in splenocytes. **e** Expression level of CD40 on DCs in splenocytes. Data represent the mean±standard deviation ($n \geq 3$). *$p<0.05$ was used to indicate significant differences

systemic mucosal immune system. This experiment shows that ultrasonic treatment not only induced the production of the same IgG, IgG1 and IgG2a antibody titers as the other groups but also induced an immune response that is a mixed or balanced Th1 and Th2 immune response. In particular, the MnO_2@COS@OVA particles enhance the systemic mucosal immune response after ultrasonic treatment.

In vitro stimulation of splenocytes to secrete cytokines

The level of cytokines secreted by splenocytes is an important indicator of the strength and type of immune response. Mature DCs deliver antigens to $CD4^+$ or $CD8^+$ T cells via MHC II or MHC I molecules to mediate humoral or cellular immunity, respectively. Then, the Th1 subpopulation of $CD4^+$ T cells secretes cytokines such as TNF-α and IFN-γ to promote the production of cytotoxic T lymphocytes by $CD8^+$ T cells. The Th2 subpopulation of $CD4^+$ T cells secretes cytokines such as IL-4 and IL-6 to promote the activation and proliferation of B cells [43–45]. We investigated whether ultrasound-treated vaccine preparations could promote the secretion of splenocyte cytokines. ELISA kits were used to detect four cytokines, IFN-γ, TNF-α, IL-4 and IL-6, in the supernatant. As shown in Figs. 8a–8d, the MnO_2@COS@OVA+US group induction of IFN-γ secretion by splenocytes in vitro is higher than those of the remaining four groups. The induction of TNF-α and IL-6 secretion by splenocytes in vitro was significantly higher in the MnO2@COS@OVA+US group than in the other three groups (OVA, MnO_2@COS@OVA and MnO_2@COS@OVA-SC). The induction of IL-4 secretion by splenocytes in the MnO2@COS@OVA+US group was significantly higher than that in the other three groups (OVA, Alum@OVA and MnO_2@COS@OVA). This experiment shows that MnO_2@COS@OVA particles induced a better Th1-type immune response and Th2-type immune response after ultrasound treatment. This result is basically consistent with the results of antibody potency analysis.

Activation of memory T cells

The adaptive immune system can record unique antigen characteristics and establish immune memory after the first appearance of an antigen. When the same antigen is re-exposed, memory T cells can respond rapidly to clear the antigen [46, 47]. Memory T cells can be divided into effector memory T cells ($CD44^{high}CD62L^{low}$) and central memory T cells ($CD44^{high}CD62L^{high}$). Effector memory T cells are distributed in lymphoid and nonlymphoid tissues and can induce cytokine secretion to initiate immune protection and rapid effector functions [48]. To investigate whether the ultrasound-treated vaccine preparation promoted the activation of memory T cells, the collected splenocytes were stained with fluorescently labeled antibody

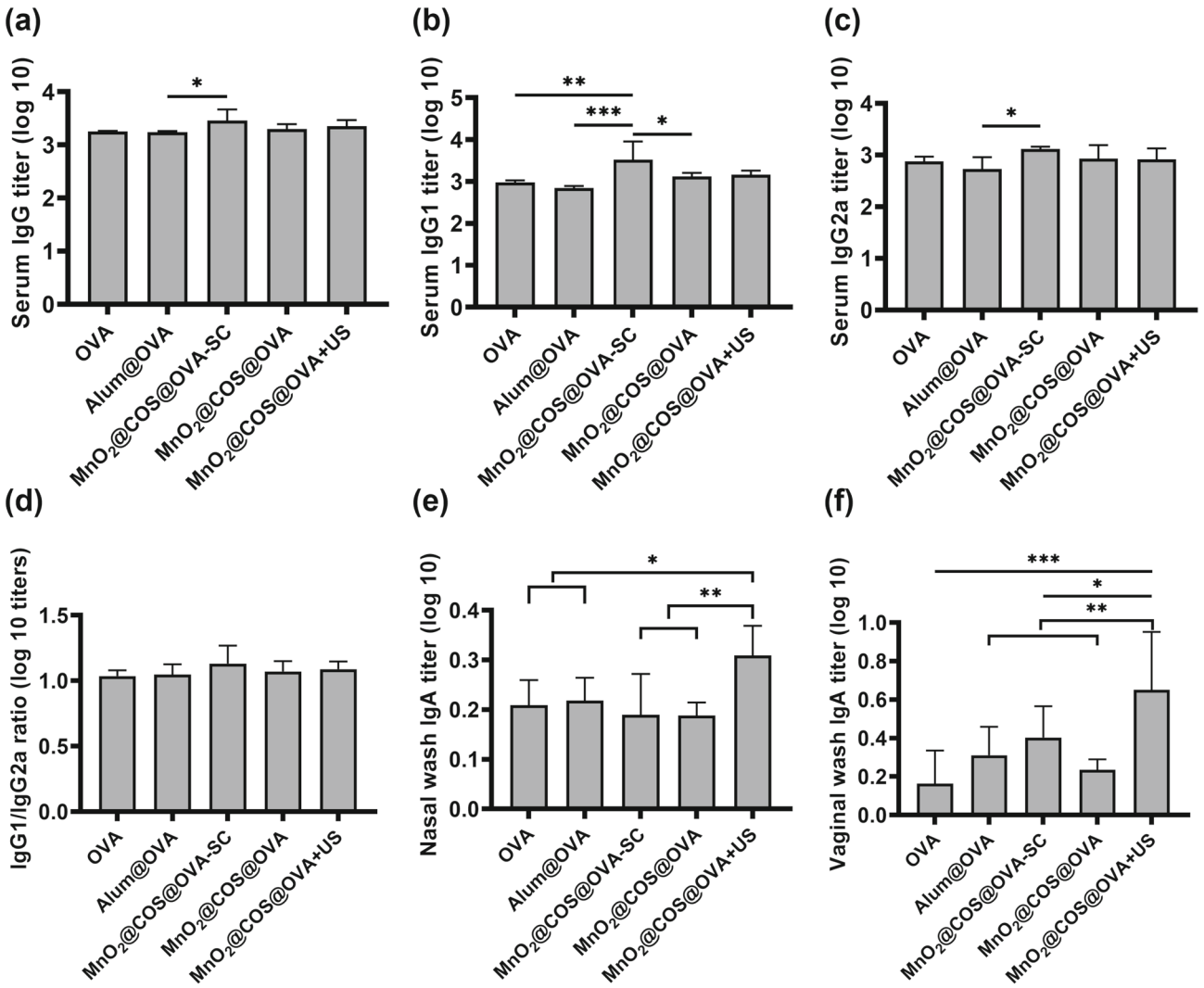

Fig. 7 OVA allosteric antibody secretion after immunization of mice with different vaccine preparations and treatments. **a** IgG secretion level. **b** IgG1 secretion level. **c** IgG2a secretion level. **d** IgG1/IgG2a ratio. **e** Nasal IgA secretion level. **f** IgA secretion level in the genital tract. Data represent the mean±standard deviation ($n \geq 3$). *$p<0.05$, **$p<0.01$, and ***$p<0.001$ were used to indicate significant differences

reagents, and the results were analyzed by flow cytometry. As shown in Figs. 9a–9c, the expression levels of $CD44^{high}CD62L^{low}$ in $CD4^+$ T cells and $CD8^+$ T cells in the MnO_2@COS@OVA+US group were significantly higher than those in the remaining four groups. This experiment shows that mice in the MnO_2@COS@OVA+US group can rapidly develop humoral and cellular immunity when re-exposed to the same antigen.

Systemic toxicity analysis

The heart, liver, spleen, lung, and kidney of each group of mice were extracted, and the resulting organs were made into tissue sections and subjected to HE staining to determine the issue of systemic toxicity of the vaccine by observing the cellular morphology. As shown in Fig. 10, the two groups containing MnO_2 in the vaccine adjuvant had intact cell morphology in their tissue sections with no obvious damage. This indicates the absence of serious toxic effects of the vaccine.

Conclusions

This study shows that ultrasound treatment promotes the penetration of MnO_2@COS@OVA particles into the superficial layer of the nasal mucosa and promotes the recruitment of DCs and macrophages, as well as the infiltration of T cells in the nasal mucosal tissue. After ultrasound treatment, MnO_2@COS@OVA particles promote the maturation of DCs and the formation of $CD4^+$ and $CD8^+$ effector

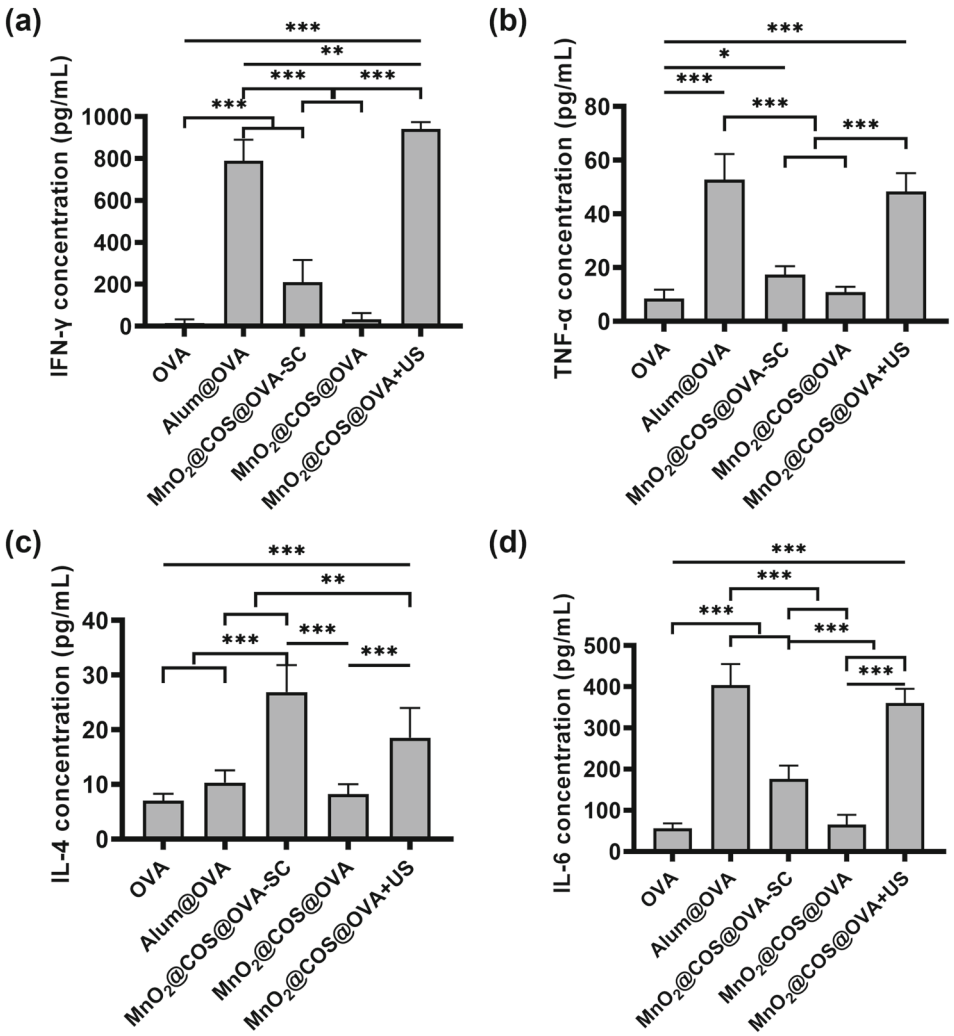

Fig. 8 Stimulated splenocytes to secrete cytokines in vitro. **a** The level of IFN-γ secretion. **b** The level of TNF-α secretion. **c** The level of IL-4 secretion. **d** The level of IL-6 secretion. Data represent the mean±standard deviation ($n \geq 3$). *$p<0.05$, **$p<0.01$, and ***$p<0.001$ were used to indicate significant differences

memory T cells in vivo and ex vivo. It also promotes the secretion of cytokines from splenocytes in vitro, which produces better cellular and humoral immunity. In addition, MnO_2@COS@OVA particles have good biocompatibility and do not cause significant damage to nasal mucosal tissues and vital organs in vivo. In particular, after ultrasound treatment, MnO_2@COS@OVA particles increased the level of secretory IgA antibodies in the mucosa of the nasal cavity and genital tract of mice and induced an effective anti-OVA-specific mucosal immune response. This experiment shows that MnO_2@COS@OVA particles induce a stronger systemic mucosal immune response after ultrasonic treatment. In recent years, viral and bacterial infections as well as mucosal cancer have been medical problems that the world needs to overcome, and ultrasound treatment can promote mucosal vaccines to induce an efficient immune mucosal response, which provides new ideas to solve these problems.

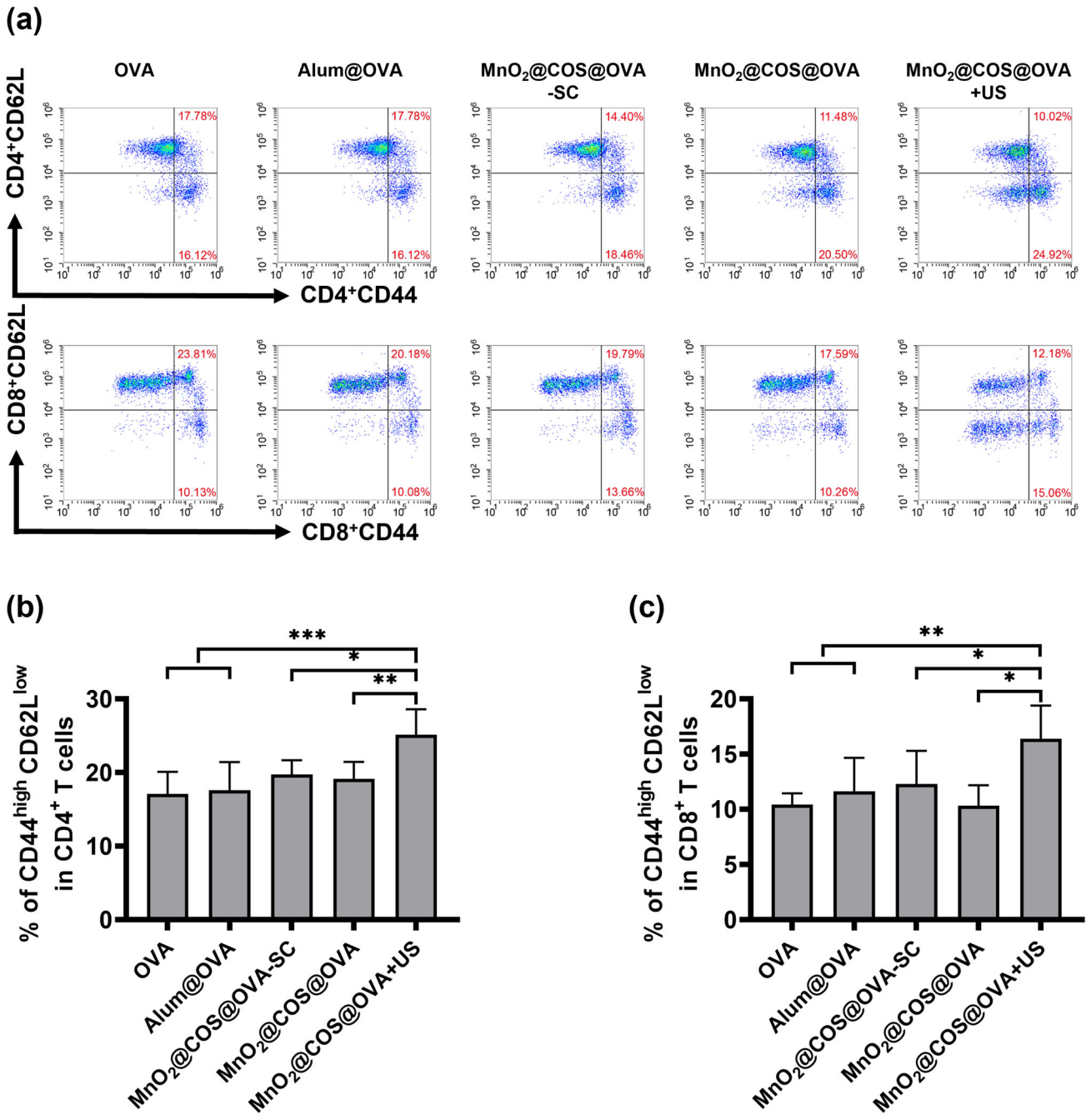

Fig. 9 **a** The percentage of effector ($CD44^{high}CD62L^{low}$) memory T cells in $CD4^+$ and $CD8^+$ T cells was detected by using a flow cytometer. **b** The percentage of $CD4^+CD44^{high}CD62L^{low}$ effector memory T cells in spleen cells. **c** The percentage of $CD8^+CD44^{high}CD62L^{low}$ effector memory T cells in spleen cells. Data represent the mean±standard deviation ($n \geq 3$). *$p<0.05$, **$p<0.01$, and ***$p<0.001$ were used to indicate significant differences

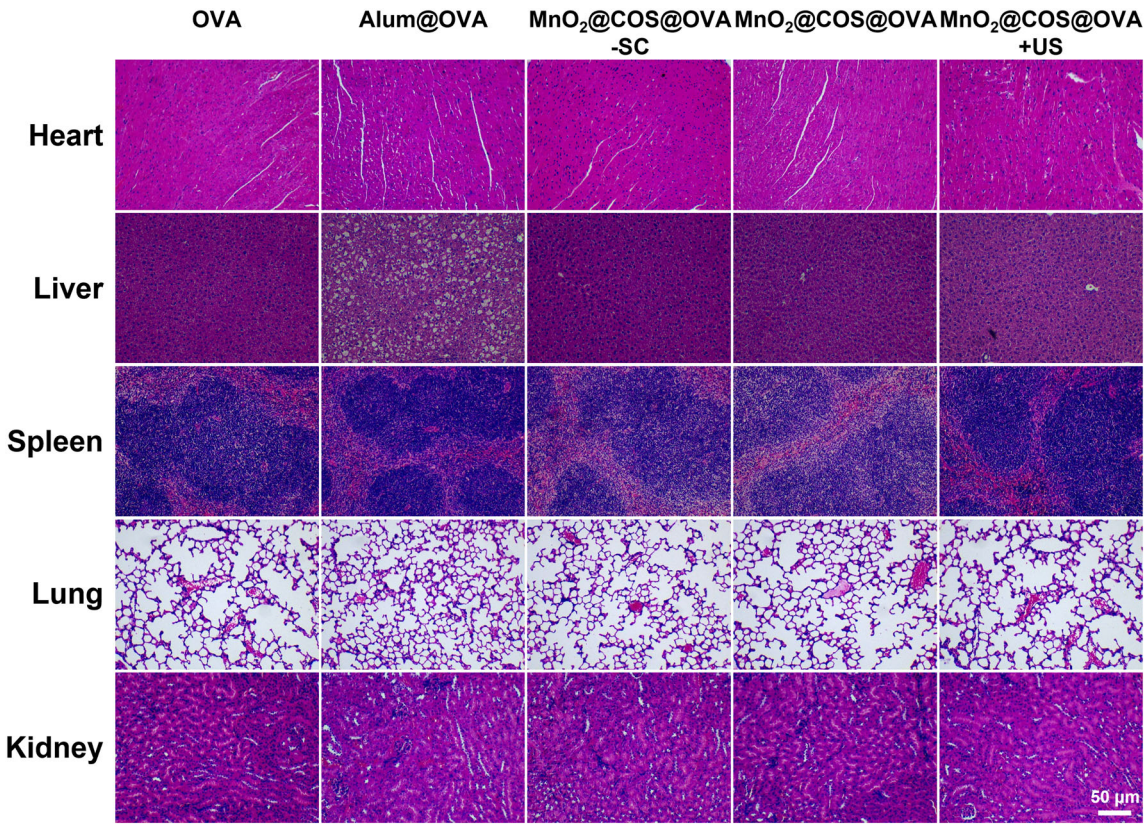

Fig. 10 Toxicity of different vaccine preparations and treatments on organs in vivo. HE staining plots of major organs in five groups of animals with OVA, Alum@OVA, MnO_2@COS@OVA-SC, MnO_2@COS@OVA, and MnO_2@COS@OVA+US, showing the damage caused by different vaccine preparations and treatments on major organs in vivo

Supplementary Information The online version contains supplementary material available at https://doi.org/10.1007/s42242-023-00231-9.

Acknowledgements This work was supported by the National Key R&D Program of China (No. 2018YFC0311103).

Author contributions HWX: conceptualization, investigation, writing—original draft. YL: methodology, formal analysis, data curation. MS: validation. DGY: resources. HBW: supervision, funding acquisition, validation. ZHL: project administration, funding acquisition, writing—review & editing.

Declarations

Conflict of interest The authors declare that they have no conflict of interest.

Ethical approval All animal experiments in this study followed animal ethics and Jinan University guidelines (Ethics Approval Number: 20211116-04).

References

1. Neutra MR, Pringault E, Kraehenbuhl JP (1996) Antigen sampling across epithelial barriers and induction of mucosal immune responses. Annu Rev Immunol 14:275–300. https://doi.org/10.1146/annurev.immunol.14.1.275
2. Chase C, Kaushik RS (2019) Mucosal immune system of cattle all immune responses begin here. Vet Clin N Am Food A 35(3):431–451. https://doi.org/10.1016/j.cvfa.2019.08.006
3. Marasini N, Skwarczynski M, Toth I (2017) Intranasal delivery of nanoparticle-based vaccines. Ther Deliv 8(3):151–167. https://doi.org/10.4155/tde-2016-0068
4. Feng F, Wen Z, Chen J et al (2022) Strategies to develop a mucosa-targeting vaccine against emerging infectious diseases. Viruses 14(3):520. https://doi.org/10.3390/v14030520
5. Wang M, Zhang Y, Pan L (2014) Advance in attenuated salmonella vector on intestinal mucosal immunity. Chin Vet Sci 44(1):104–110
6. Yu Q, Zhu L, Kang H et al (2013) Mucosal lactobacillus vectored vaccines. Hum Vaccin Immunother 9(4):805–807. https://doi.org/10.4161/hv.23302
7. Jiang PL, Lin HJ, Wang HW et al (2015) Galactosylated liposome as a dendritic cell-targeted mucosal vaccine for inducing protective anti-tumor immunity. Acta Biomater 11:356–367. https://doi.org/10.1016/j.actbio.2014.09.019
8. Huang CH, Huang CY, Ho HM et al (2020) Nanoemulsion adjuvantation strategy of tumor-associated antigen therapy rephrases mucosal and immunotherapeutic signatures following intranasal vaccination. J Immunother Cancer 8(2):e001022. https://doi.org/10.1136/jitc-2020-001022
9. Clow F, Peterken K, Pearson V et al (2020) Pilvax, a novel lactococcus lactis-based mucosal vaccine platform, stimulates systemic and

mucosal immune responses to staphylococcus aureus. Immunol Cell Biol 98(5):369–381. https://doi.org/10.1111/imcb.12325
10. Marasini N, Skwarczynski M, Toth I (2014) Oral delivery of nanoparticle-based vaccines. Expert Rev Vaccines 13(11):1361–1376. https://doi.org/10.1586/14760584.2014.936852
11. Csaba N, Garcia-Fuentes M, Alonso MJ (2009) Nanoparticles for nasal vaccination. Adv Drug Deliv Rev 61(2):140–157. https://doi.org/10.1016/j.addr.2008.09.005
12. Zaman M, Chandrudu S, Toth I (2013) Strategies for intranasal delivery of vaccines. Drug Deliv Transl Res 3(1):100–109. https://doi.org/10.1007/s13346-012-0085-z
13. Ter Haar G (1999) Therapeutic ultrasound. Eur J Ultrasound 9(1):3–9. https://doi.org/10.1016/s0929-8266(99)00013-0
14. Ferrara K, Pollard R, Borden M (2007) Ultrasound microbubble contrast agents: fundamentals and application to gene and drug delivery. Annu Rev Biomed Eng 9:415–447. https://doi.org/10.1146/annurev.bioeng.8.061505.095852
15. Mitragotri S (2005) Healing sound: the use of ultrasound in drug delivery and other therapeutic applications. Nat Rev Drug Discov 4(3):255–260. https://doi.org/10.1038/nrd1662
16. Zhu WJ, Chen Q, Jin QT et al (2021) Sonodynamic therapy with immune modulatable two-dimensional coordination nanosheets for enhanced anti-tumor immunotherapy. Nano Res 14(1):212–221. https://doi.org/10.1007/s12274-020-3070-8
17. Garcia-Gradilla V, Sattayasamitsathit S, Soto F et al (2014) Ultrasound-propelled nanoporous gold wire for efficient drug loading and release. Small 10(20):4154–4159. https://doi.org/10.1002/smll.201401013
18. Yudina A, Lepetit-Coiffe M, Moonen CT (2011) Evaluation of the temporal window for drug delivery following ultrasound-mediated membrane permeability enhancement. Mol Imaging Biol 13(2):239–249. https://doi.org/10.1007/s11307-010-0346-5
19. Wang JJ, Liu XY, Qi YF et al (2021) Ultrasound-propelled nanomotors for improving antigens cross-presentation and cellular immunity. Chem Eng J 416:129091. https://doi.org/10.1016/j.cej.2021.129091
20. Labarca CC, Makhutu M, Lumsdon AE et al (2015) The adjuvant effect of low frequency ultrasound when applied with an inactivated *Aeromonas salmonicida* vaccine to rainbow trout (*Oncorhynchus mykiss*). Vaccine 33(11):1369–1374. https://doi.org/10.1016/j.vaccine.2015.01.027
21. Li XF, Khorsandi S, Wang YF et al (2022) Cancer immunotherapy based on image-guided sting activation by nucleotide nanocomplex-decorated ultrasound microbubbles. Nat Nanotechnol 17(8):891–899. https://doi.org/10.1038/s41565-022-01134-z
22. Wang S, Hu Z, Wang XL et al (2014) 5-aminolevulinic acid-mediated sonodynamic therapy reverses macrophage and dendritic cell passivity in murine melanoma xenografts. Ultrasound Med Biol 40(9):2125–2133. https://doi.org/10.1016/j.ultrasmedbio.2014.05.007
23. Tezel A, Paliwal S, Shen ZC et al (2005) Low-frequency ultrasound as a transcutaneous immunization adjuvant. Vaccine 23(29):3800–3807. https://doi.org/10.1016/j.vaccine.2005.02.027
24. Yang GB, Xu LG, Chao Y et al (2017) Hollow MnO_2 as a tumor-microenvironment-responsive biodegradable nano-platform for combination therapy favoring antitumor immune responses. Nat Commun 8:902. https://doi.org/10.1038/s41467-017-01050-0
25. Zhang R, Wang CG, Guan YK et al (2021) Manganese salts function as potent adjuvants. Cell Mol Immunol 18(5):1222–1234. https://doi.org/10.1038/s41423-021-00669-w
26. Pawar D, Goyal AK, Mangal S et al (2010) Evaluation of mucoadhesive plga microparticles for nasal immunization. AAPS J 12(2):130–137. https://doi.org/10.1208/s12248-009-9169-1
27. Fromen CA, Robbins GR, Shen TW et al (2015) Controlled analysis of nanoparticle charge on mucosal and systemic antibody responses following pulmonary immunization. Proc Natl Acad Sci USA 112(2):488–493. https://doi.org/10.1073/pnas.1422923112
28. Ferber S, Gonzalez RJ, Cryer AM et al (2020) Immunology-guided biomaterial's design as mucosal cancer vaccine. Adv Mater 32(13):1903847. https://doi.org/10.1002/adma.201903847
29. Xing L, Zhou TJ, Fan YT et al (2019) Efficient mucosal immunization by mucoadhesive and ph-sensitive polymeric vaccine delivery system. Macromol Res 27(3):215–226. https://doi.org/10.1007/s13233-019-7042-3
30. Zhang TR, Zhang Q, Ge JP et al (2009) A self-templated route to hollow silica microspheres. J Phys Chem C 113(8):3168–3175. https://doi.org/10.1021/jp810360a
31. Pires A, Fortuna A, Alves G et al (2009) Intranasal drug delivery: how, why and what for? J Pharm Pharm Sci 12(3):288–311. https://doi.org/10.18433/J3nc79
32. Tezel A, Sens A, Tuchscherer J et al (2001) Frequency dependence of sonophoresis. Pharm Res 18(12):1694–1700. https://doi.org/10.1023/a:1013366328457
33. Guan X, Chen J, Hu Y et al (2018) Highly enhanced cancer immunotherapy by combining nanovaccine with hyaluronidase. Biomaterials 171:198–206. https://doi.org/10.1016/j.biomaterials.2018.04.039
34. Han TL, Zhang XM, Fu XQ et al (2017) Facile synthesis of chitosan nanoparticle-modified MnO_2 nanoflakes for ultrafast adsorption of pb(II) from aqueous solution. Water Supply 17(1):32–38. https://doi.org/10.2166/ws.2016.109
35. Haris PI, Severcan F (1999) Ftir spectroscopic characterization of protein structure in aqueous and non-aqueous media. J Mol Catal B Enzym 7(1–4):207–221. https://doi.org/10.1016/S1381-1177(99)00030-2
36. Cone RA (2009) Barrier properties of mucus. Adv Drug Del Rev 61(2):75–85. https://doi.org/10.1016/j.addr.2008.09.008
37. Mora JR, von Andrian UH (2006) T-cell homing specificity and plasticity: new concepts and future challenges. Trends Immunol 27(5):235–243. https://doi.org/10.1016/j.it.2006.03.007
38. Lv M, Li S, Zhao HJ et al (2017) Redox-responsive hyperbranched poly(amido amine) and polymer dots as a vaccine delivery system for cancer immunotherapy. J Mater Chem B 5(48):9532–9545. https://doi.org/10.1039/c7tb02334k
39. Van De Laar L, Coffer PJ, Woltman AM (2012) Regulation of dendritic cell development by GM-CSF: molecular control and implications for immune homeostasis and therapy. Blood 119(15):3383–3393. https://doi.org/10.1182/blood-2011-11-370130
40. Dobrovolskaia MA, McNeil SE (2016) Immunological properties of engineered nanomaterials: an introduction. In: Dobrovolskaia MA (Ed.), Handbook of Immunological Properties of Engineered Nanomaterials vol. 1, pp. 1-24
41. Li M, Jiang YH, Xu CQ et al (2013) Enhanced immune response against HIV-1 induced by a heterologous DNA prime-adenovirus boost vaccination using mannosylated polyethyleneimine as DNA vaccine adjuvant. Int J Nanomed 8:1843–1854. https://doi.org/10.2147/Ijn.S43827
42. Wilson HL, Obradovic MR (2015) Evidence for a common mucosal immune system in the pig. Mol Immunol 66(1):22–34. https://doi.org/10.1016/j.molimm.2014.09.004

43. Li X, Wang XP, Ito A (2018) Tailoring inorganic nanoadjuvants towards next-generation vaccines. Chem Soc Rev 47(13):4954–4980. https://doi.org/10.1039/c8cs00028j
44. Paul WE, Seder RA (1994) Lymphocyte responses and cytokines. Cell 76(2):241–251. https://doi.org/10.1016/0092-8674(94)90332-8
45. Liu ZG, Xing J, Zheng SS et al (2016) Ganoderma lucidum polysaccharides encapsulated in liposome as an adjuvant to promote th1-bias immune response. Carbohydr Polym 142:141–148. https://doi.org/10.1016/j.carbpol.2016.01.021
46. Fearon DT, Manders P, Wagner SD (2001) Arrested differentiation, the self-renewing memory lymphocyte, and vaccination. Science 293(5528):248–250. https://doi.org/10.1126/science.1062589
47. Kinjo Y, Kronenberg M (2005) Vα14i NKT cells are innate lymphocytes that participate in the immune response to diverse microbes. J Clin Immunol 25(6):522–533. https://doi.org/10.1007/s10875-005-8064-5
48. Okazaki S, Iwasaki T, Yuba E et al (2018) Evaluation of ph-sensitive fusogenic polymer-modified liposomes co-loaded with antigen and α-galactosylceramide as an anti-tumor vaccine. J Vet Med Sci 80(2):197–204. https://doi.org/10.1292/jvms.17-0491